Gusseted rafter-to-column connections of double-bay single channel portal frames

B. Tshuma & M. Dundu
Department of Civil Engineering Science, University of Johannesburg, P O Box 524, Auckland Park 2006, South Africa

ABSTRACT: Double-bay portal frames have several advantages over two single portal frames positioned adjacent to each other, however the connecting system can be a challenge, especially if the portal frame is formed from single cold-formed channels. The portal frames described in this paper consists of a column and two rafter members, formed from single cold-formed channels sections, and bolted back-to-back at the eaves joint through a gusset plate. Tests were performed to evaluate the structural performance of the eaves region of double-bay portal frames. The eaves region represents the distance from the point of maximum moment (eaves joint) to the point of zero moment (contraflexure) in the rafters and columns respectively. The structures failed by local buckling in the compression flange and web of the rafters, outside the joints. The moment-curvature graphs proved that plasticity could not be achieved in these connections.

1 INTRODUCTION

Double-bay portal frames optimises the existence of two single portal frames positioned adjacent to each other, however, it is not easy to develop the configuration of the internal eaves connection. Although most aspects of the behaviour and design of double-bay portal frames are similar to single-bay structures, the design of the internal eaves connections is different. This study reports on the structural performance of an internal eaves connection of a double-bay portal frame, consisting of two single channel cold-formed rafters connected back-to-back to the column, through hot-rolled steel gusset plates, as shown in Figure 1.

The eaves connections use a total of 12, M20 bolts and either 6 mm or 8 mm thick hot-rolled steel gusset plate. The connection of the rafters to the gusset plate at the same level eliminates the column moments, allowing the column to be designed for compression forces only, under vertical downward loading. The span, spacing and eaves height of the frames investigated is 12 m, 4.5 m and 3 m, respectively. These dimensions are derived from a previous study by Dundu (2003).

2 MATERIAL PROPERTIES

A summary of the average material properties of cold-formed steel channels and hot-rolled steel gusset plates is shown in Table 1.

Table 1. Average material properties of cold-formed steel channels and hot-rolled steel gusset plates

Channel section	Specimen	f_y	f_u	E
		MPa	MPa	GPa
300 × 75 × 20 × 3	LWC	240.828	321.256	207
	LFC	253.900	331.654	
	LCC	366.885	406.089	
300 × 65 × 20 × 3	LWC	228.666	309.215	206
	LFC	240.330	317.852	
	LCC	322.244	375.391	
300 × 50 × 20 × 3	LWC	255.153	335.048	208
	LFC	330.550	367.675	
	LCC	379.962	402.319	
6 mm gusset plate	LC	342.754	463.619	201
8 mm gusset plate	LC	351.865	496.859	200

Coupons (longitudinal web coupons (LWC), longitudinal flange coupons (LFC), longitudinal corner coupons (LCC) and longitudinal coupons (LC)) were tested to evaluate the material properties of each channel and gusset plate. The coupons were prepared and tested in accordance with the guidelines provided by ISO 6892-1 (2009). The Young's modulus of elasticity (E) of each channel was established from averaging the slope of the stress-strain curve of its respective coupons over the elastic region.

Material properties tests on bolts were not done since the strength of the bolts ($f_u \geq 800$ MPa) is less critical than the bearing strength of cold-formed steel channels and hot-rolled steel gusset plates.

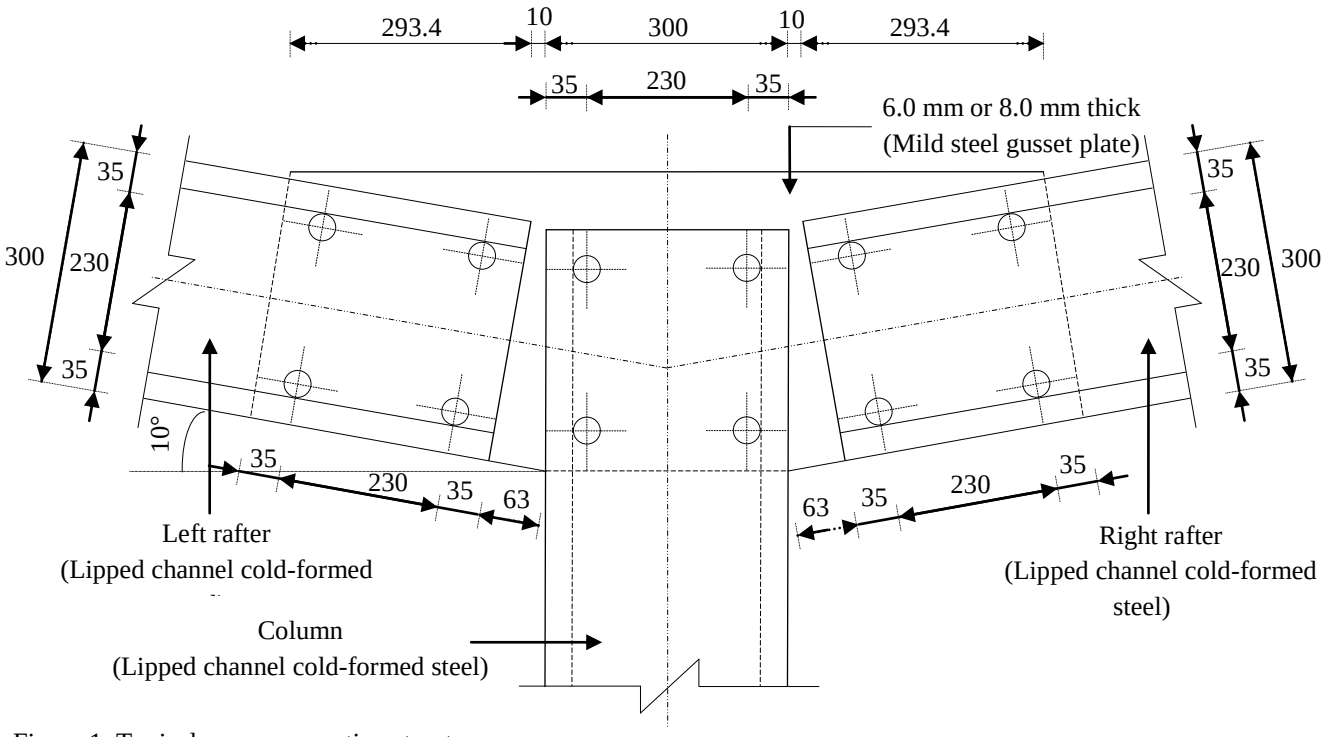

Figure 1. Typical eaves connection structure

3 EXPERIMENTAL INVESTIGATION

3.1 *Test model*

To simplify the experimental work, only the region around the internal eaves connection was tested. A total of six frames were tested (three eaves connection type 1 (ECT-1) structures and three eaves connection type 2 (ECT-2) structures). Three variables were investigated, and these are the width of the channel flanges, the thickness of the gusset plate (t_g) (Table 2) and the material properties of the cold-formed steel channels (Table 1).

3.2 *Structure details and instrumentation*

The layout and geometry of ECT-1 and ECT-2 structures is shown in Figure 2. Both ECT-1 and ECT-2 have three joints namely; the gusset plate-to-column joint (J), the left rafter-to-gusset plate joint (I) and the right rafter-to-gusset plate joint (K). Points H and L are the load application points in the left and right rafters, respectively.

Table 2. Variables in the tested structures

Structure No.	Chanel size	t_g
		mm
ECT-1.1	300 × 75 × 20 × 3	6
ECT-1.2	300 × 65 × 20 × 3	6
ECT-1.3	300 × 50 × 20 × 3	6
ECT-2.1	300 × 75 × 20 × 3	8
ECT-2.2	300 × 65 × 20 × 3	8
ECT-2.3	300 × 50 × 20 × 3	8

Point M is the load application point in the column for both rafters and point N is the column base. The lever arm (e) represents the perpendicular distance from the gusset plate-to-column joint to the applied load (P). The elevated testing platform (1.52m high) and rafter restraint columns were mounted onto the mild steel base plates and bolted to the laboratory floor.

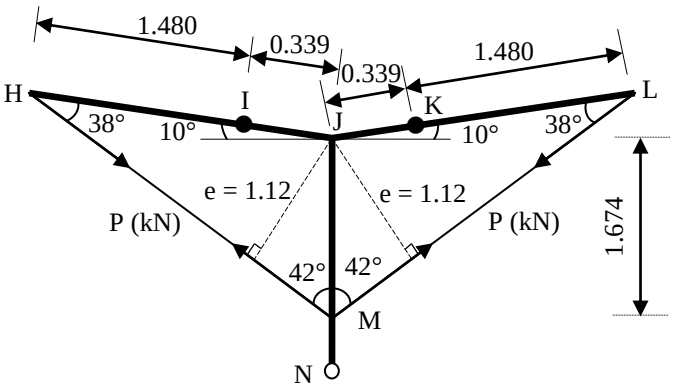

Figure 2. Layout and geometry of ECT-1 and ECT-2 structures

The test frames were assembled on the laboratory floor and lifted into the elevated test platform using a crane. Lateral-torsional buckling of the rafters was controlled by column restraints. Alwayse ball transfer units were installed on the restraint columns to facilitate a frictionless movement of the rafters during the test.

Electronic clinometers and strain gauges were used to measure joints rotations and strains, respectively. The load was applied equally and simultaneously to the rafters using two, hand-held, 10 ton hydraulic jacks.

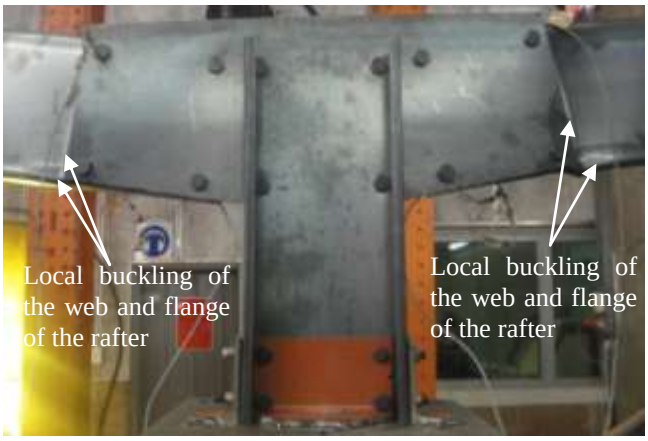

Figure 3. Typical local buckling failure in all tested structures

3.3 *Test procedure*

Before testing, all the test instruments and software were checked to ensure that they are working properly. Both rafters were subjected to simultaneous equal loads to simulate the actual loading conditions of the portal frame. Load increments of 0.5 kN at two minutes intervals were applied up to ninety percent of the expected failure load. Thereafter, the loading interval was increased to three minutes. This was done to observe the failure modes of the frames. Joint rotations and strains were monitored through a data logger. Applied loads were recorded and stored in the load display software. At the end of each test, the structure members were disassembled and bolt-hole elongations measured and recorded.

4 FAILURE MODES

All the structures failed by local buckling of the web of the rafters, immediately outside the gusset plate-rafter joints. Subsequently, the compression flange also failed, as shown in Figure 3. As expected, the gusset plate-to-column connection did not fail since it is subjected to axial forces only. Bearing deformations were observed in the bolt-holes, and did contribute to the failure of the rafters.

5 THEORETICAL & EXPERIMENTAL RESULTS

A comparison of the theoretical and experimental results is shown in Table 3. The yield moment (M_y), axial load (N_y) and shear resistance (V_r) of the cold-formed steel channels are calculated from the effective cross-sectional properties of the channels, to allow for local buckling. The maximum moment (M_{ux}), axial forces (N_{max}) and shear forces (V_{max}) are calculated using the layout and geometry shown in Figure 2. In all the tests performed, the capacities of the frames are lower than the theoretical elastic resistances of the cold-formed channels. The frames only achieved between 15% and 18% of the axial load (N_y) and between 14% and 17% of the shear resistance (V_r) of the cold-formed steel channels. ECT-1 and ECT-2 structures produced maximum moments (M_{ux}) between 76% and 86% and between 88% and 93% of the yield moment (M_y) of the cold-formed channels (Table 4).

5.1 *Joint resistances*

In all the tested structures, the joints did not fail. This suggests that the connections were not the critical part in these tests. In order to relate the capacity of the connections to the capacity of the frames, the theoretical moment of resistance of the connections (M_{rj}), is computed using the bearing resistance (B_r) of the channel, since this is more critical than the shearing resistance of the bolts (V_{rb}). The B_r and the V_{rb} are determined from Equation 1 and 2.

$$B_r = atf_u \leq Cdtf_u \quad (1)$$

$$V_{rb} = 0.7 \times 0.60nmA_b f_{ub} \quad (2)$$

where a = distance from the bolt-hole centre to the edge, in the direction of the force; t = minimum thickness of the connected parts; f_u = minimum tensile strength of the channel; C = bearing resistance factor of fasteners (Kemp (2001); d = nominal diameter of the fastener; n = number of bolts; A_b = cross-sectional area of bolt based on nominal diameter; and m = number of faying surfaces or shear planes in a bolted joint; f_{ub} = tensile strength of the bolt. 0.7 is used since the bolts are fully threaded and 0.6 converts the tensile stress into a shear stress.

The theoretical moment of resistance of the joints (M_{rj}) is calculated from the bearing resistance (B_r) and the lever arm (e) of each bolt in the connection. Table 4 shows the comparison of ultimate and yield moments and theoretical moment of resistance of connections. As indicated in section 4, the strength of the frames was governed by local buckling of the channels. This agrees with the results of most connections in Table 4. Although the maximum moment (M_{ux}), and the theoretical moment of resistance of the connections (M_{rj}) of connections ECT-2.1 and ECT-2.2 seem to suggest that the connections were more critical, this was not the case. A ratio of M_{ux} to M_{rj} of almost 1 implies that the joints were just about to fail when the rafters failed by local buckling. Structures formed from 8mm gusset plates produced higher ratios of M_{ux} to M_{rj} compared to those formed from 6mm gusset plates. This was probably caused by the small lateral deflection experienced by the 6mm gusset plates.

Table 3. Comparison of theoretical and experiment results

Structure No.	Channel size	Theoretical results			Experiment results		
		M_y	N_y	V_r	M_{ux}	N_{max}	V_{max}
		kNm	kN	kN	kNm	kN	kN
ECT-1.1	300 × 75 × 20 × 3	28.15	236.48	94.13	21.42	34.93	14.47
ECT-1.2	300 × 65 × 20 × 3	24.72	212.84	91.50	21.23	34.63	14.34
ECT-1.3	300 × 50 × 20 × 3	24.09	209.79	95.10	19.51	31.82	13.18
ECT-2.1	300 × 75 × 20 × 3	28.15	236.48	94.13	24.83	40.50	16.78
ECT-2.2	300 × 65 × 20 × 3	24.72	212.84	91.50	23.05	37.59	15.57
ECT-2.3	300 × 50 × 20 × 3	24.09	209.79	95.10	21.63	35.27	14.61

Table 4. Comparison of ultimate and yield moments and theoretical moment of resistance of joints

Structure No.	Channel size	f_y	f_u	P	e	M_{ux}	M_y	M_{ux}/M_y	B_r	M_{rj}	M_{ux}/M_{rj}
		MPa	MPa	kN	m	kNm	kNm		kN	kNm	
ECT-1.1	300 × 75 × 20 × 3	240.828	321.256	23.50	0.91	21.42	28.15	0.76	34.70	22.57	0.95
ECT-1.2	300 × 65 × 20 × 3	228.666	309.215	23.30	0.91	21.23	24.72	0.86	33.40	21.72	0.98
ECT-1.3	300 × 50 × 20 × 3	255.153	335.048	21.41	0.91	19.51	24.09	0.81	36.19	23.53	0.83
ECT-2.1	300 × 75 × 20 × 3	240.828	321.256	27.25	0.91	24.83	28.15	0.88	34.70	22.57	1.10
ECT-2.2	300 × 65 × 20 × 3	228.666	309.215	25.29	0.91	23.05	24.72	0.93	33.40	21.72	1.06
ECT-2.3	300 × 50 × 20 × 3	255.153	335.048	23.73	0.91	21.63	24.09	0.90	36.19	23.53	0.92

Table 5. Average maximum moment, rotation, joint rotational stiffness and curvature results at rafter failure

Structure No.	Channel size	f_y	M_{ux}	ϕ_{max}	ϕ_{sj}	K_{max}
		MPa	kNm	Rad.	kNm/rad	(1/mm) 10E-6
ECT-1.1	300 × 75 × 20 × 3	240.828	21.42	0.016	1338.75	5.95
ECT-1.2	300 × 65 × 20 × 3	228.666	21.23	0.018	1179.44	6.26
ECT-1.3	300 × 50 × 20 × 3	255.153	19.51	0.015	1300.67	6.18
ECT-2.1	300 × 75 × 20 × 3	240.828	24.83	0.012	2069.17	7.67
ECT-2.2	300 × 65 × 20 × 3	228.666	23.05	0.013	1773.08	6.52
ECT-2.3	300 × 50 × 20 × 3	255.153	21.63	0.009	2403.33	6.33

The reason why the capacities of the both ECT-1 and ECT-2 structures are almost the same is that all the connections did not fail. However, the rafters failed by local buckling of the compression web and flange.

The width of the cold-formed steel channel flanges and the thickness of the hot-rolled gusset plates influenced the ultimate moments more than the material properties of the cold-formed channels. Structures formed from the 300 × 75 × 20 × 3 channel section produced the highest ultimate moments, followed by the 300 × 65 × 20 × 3 channel, and the least ultimate moments were produced by the 300 × 50 × 20 × 3 channel.

ECT-1 structures are significantly ductile but less stiff than ECT-2 structures. On the other hand, ECT-2 structures are significantly stiff but less ductile compared to ECT-1 structures. It can thus be concluded that connections formed from small thickness gusset plates of lower material strength can be reasonably ductile but less stiff than connections formed from thick gusset plates of high material strength. The latter connection is significantly stiff but less ductile.

The average secant rotational stiffnesses of the joints (ϕ_{sj}) shown in Table 5 are obtained by dividing the maximum moment (M_{ux}) by the maximum joint rotation (ϕ_{max}), at rafter failure. The ϕ_{sj}, at rafter failure, show that frames that obtained high joint rotations, are less stiff than those with low joint rotations. Therefore, it can be seen that significantly ductile frames are less stiff than less ductile frames and vice-versa.

5.2 *Moment-rotation and curvature curves*

The average moment-rotation and curvature curves are shown in Figure 4 and Figure 5 respectively. The average moment-rotation curves for all the tested structures show negligible rotation at the initial loading stage as the load was carried by the frictional resistance between the connected members. Thereafter, the curves show a linear gradient of the moment-rotation relationships up to levels close to ultimate moment. The graphs show that ECT-2 frames are stiff and less ductile while ECT-1 frames are ductile and less stiff. This is attributed to the material properties and thickness of the gusset plates used.

The average moment-curvature curves of all the tested frames show a linear range followed by a non-linear range.

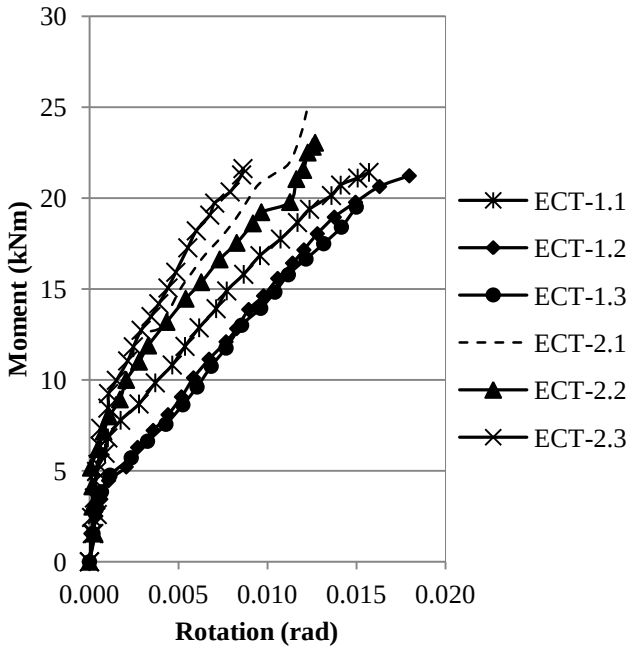

Figure 4. Average moment-rotation curves

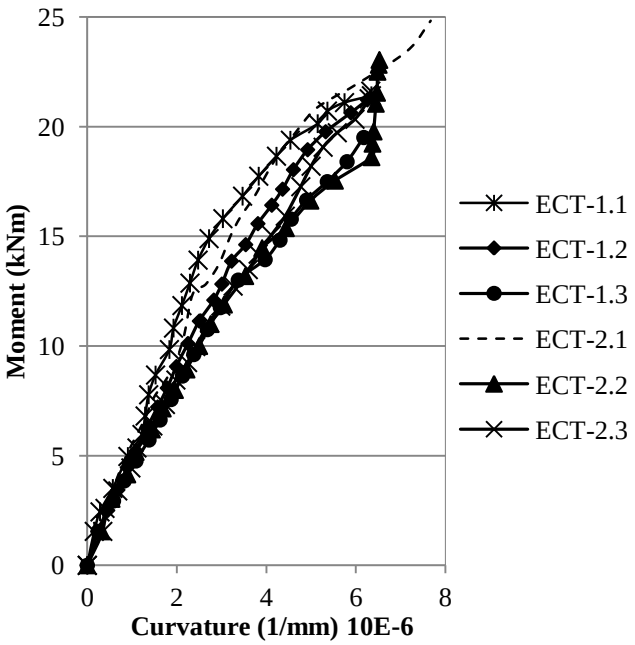

Figure 5. Average moment-curvature curves

The average moment-curvature curves illustrates that enough plasticity could not be achieved in all the channels since all structures failed within the inelastic range.

6 CONCLUSION

The investigation shows that the eaves connection of double-bay portal frame(s) formed from cold-formed steel channels connected back-to-back, through a hot-rolled steel gusset plate can be a viable connection configuration.

In all the tested frames, the eaves joints did not fail. Local buckling of the web and flange of the rafters was the ultimate failure in all the frames. Bearing distortions were also observed in the bolt-holes of the thinner cold-formed channels, however, there was no complete bearing or tearing failure.

In all the tested frames, structures made from the 300 × 50 × 20 × 3 channel produced the least ratio of M_{ux} to M_{rj}. Frames formed from channels with wider flanges produced higher ultimate joint moments compared to those formed from channels with small flanges. ECT-2 structures produced higher maximum moments compared to ECT-1 structures as a result of the use of the stiffer 8mm thick gusset plate, which helped to limit any lateral deflection experienced by the gusset plate. The average moment-curvature graphs proved that plasticity could not be achieved in all the tested structures.

In all the tested structures, the capacity of the rafters was critical compared to the capacity of the joints. To fully understand the structural performance of the internal eaves connections, the joints must fail. Therefore, further research work is recommended in order to have a full appreciation and understanding of the behaviour of the internal eaves connections of double-bay portal frames of this nature.

REFERENCES

DIN EN 1993-1-1. Design of steel structures: Part 1.1 – General rules and rules for buildings. Brussels: *European Committee of Standardization (CEN)*: 2010-12.

Dundu, M. & Kemp, AR. 2006. Strength requirements of single cold-formed channels connected back-to-back. *Journal of Constructional Steel Research* 62: 250-261.

ISO 6892-1. 2009. Metallic materials - Tensile testing. Part 1: Method of test at room temperature. Switzerland: *International Organisation for Standardization.*

Kemp, AR. 2001. Bearing capacities and modes of failure in single-bolt lap joints. *Journal of the South African Institution of Civil Engineering* 43(1): 13-18.

SANS 10162-1. 2011. South Africa standard code of practice for the structural use of steel, Part 1 – Limit states design of hot-rolled steelwork. Pretoria: *SANS*.

SANS 10162-2. 2005. South Africa standard code of practice for the structural use of steel, Part 2 – Limit states design of cold-formed steelwork. Pretoria: *SANS*.

SANS 10162-2. 2011. South Africa standard code of practice for the structural use of steel, Part 2 – Limit states design of cold-formed steelwork. Pretoria: *SANS*.